The Journal of Physiology

J Physiol 591.21 (2013) pp 5291–5303

Influence of spiking activity on cortical local field potentials

Stephan Waldert, Roger N. Lemon and Alexander Kraskov

Sobell Department of Motor Neuroscience and Movement Disorders, UCL Institute of Neurology, London WC1N 3BG, UK

Key points

- The intra-cortical local field potential (LFP) reflects a variety of electrophysiological processes and is a fundamental signal used to enhance knowledge about neuroscience.
- For most investigations, spike-free LFPs are mandatory for valid conclusions, but spikes can contaminate LFPs and falsify findings despite low-pass filtering or other attempts to remove spiking activity from LFPs. The extent of this fundamental problem remains unclear.
- Using spikes recorded in the awake monkey, we revealed how spike amplitude, spike duration, firing rate and noise statistic influence the extent to which spikes contaminate LFPs.
- Contamination varies with these parameters and can affect LFPs down to around 10 Hz; below this it is theoretically possible but unlikely. LFP frequencies up to the (high-) gamma band can remain unaffected, but signals above must always be carefully analysed.
- We propose a method to reveal modulations in spectrograms, which also allows the detection of spike contamination, and provide a systematic guide to assess spike contamination of intra-cortical LFPs.

Abstract The intra-cortical local field potential (LFP) reflects a variety of electrophysiological processes including synaptic inputs to neurons and their spiking activity. It is still a common assumption that removing high frequencies, often above 300 Hz, is sufficient to exclude spiking activity from LFP activity prior to analysis. Conclusions based on such supposedly spike-free LFPs can result in false interpretations of neurophysiological processes and erroneous correlations between LFPs and behaviour or spiking activity. Such findings might simply arise from spike contamination rather than from genuine changes in synaptic input activity. Although the subject of recent studies, the extent of LFP contamination by spikes is unclear, and the fundamental problem remains. Using spikes recorded in the motor cortex of the awake monkey, we investigated how different factors, including spike amplitude, duration and firing rate, together with the noise statistic, can determine the extent to which spikes contaminate intra-cortical LFPs. We demonstrate that such contamination is realistic for LFPs with a frequency down to ∼10 Hz. For LFP activity below ∼10 Hz, such as movement-related potential, contamination is theoretically possible but unlikely in real situations. Importantly, LFP frequencies up to the (high-) gamma band can remain unaffected. This study shows that spike–LFP crosstalk in intra-cortical recordings should be assessed for each individual dataset to ensure that conclusions based on LFP analysis are valid. To this end, we introduce a method to detect and to visualise spike contamination, and provide a systematic guide to assess spike contamination of intra-cortical LFPs.

(Received 7 May 2013; accepted after revision 25 August 2013; first published online 27 August 2013)
Corresponding author S. Waldert: Sobell Department of Motor Neuroscience and Movement Disorders, UCL Institute of Neurology, London WC1N 3BG, UK. Email: s.waldert@ucl.ac.uk

Abbreviations BMI, brain–machine interface; ECoG, electrocorticogram; EEG, electroencephalography; EMG, electromyography; FDR, false discovery rate; LFP, local field potential; MEG, magentoencephalography; rms, root mean square; SNR, signal to noise ratio.

DOI: 10.1113/jphysiol.2013.258228

Introduction

Typical intra-cortical neuronal signals recorded with open filters (0.1 Hz–10 kHz) exhibit a $1/f^{\alpha}$ spectrum and reflect a superposition of a variety of electrophysiological processes (Buzsaki *et al.* 2012). Such broadband recordings allow for simultaneous investigation of spikes and oscillations in non-spiking activity (synaptic, gap junctions, etc.). Whereas spikes are mainly considered as the output activity of single neurons, the physiological meaning of the remaining, non-spiking signal remains of debate. Both signal components can be correlated, anti-correlated or independent. However, it has become evident that non-spiking signals can provide a source of information about behaviour (Mehring *et al.* 2003; Schalk *et al.* 2007; Waldert *et al.* 2008; Zhuang *et al.* 2010). Investigating both signal types and their relationship could not only help to better understand neuronal processes but also yield higher performance and stability in brain–machine interfaces (BMIs, Waldert *et al.* 2009).

The traditional approach to separate spiking and non-spiking signals is to use a single threshold in a frequency domain, e.g. 300 Hz (Logothetis, 2003). Signals above this threshold are used for analysis of spiking activity and the low frequency component is usually referred to as the local field potential (LFP) and assumed to be spike-free. Although this approach is widely used, the above assumption is incorrect for two main reasons: the spike shapes may contain frequency components below the chosen frequency threshold (Zanos *et al.* 2011; Zanos *et al.* 2012) and spike trains may be mistaken for low frequency oscillatory activity (Bair *et al.* 1994). Both factors result in spike contamination of LFP and possible misinterpretation of neuronal activity. Several studies have shown that increased LFP power in frequencies around 90 Hz (high-gamma) might in fact indicate high spiking activity (Quilichini *et al.* 2010; Ray & Maunsell, 2011; Belluscio *et al.* 2012; Schomburg *et al.* 2012). Spikes can contaminate the LFP in frequencies below 90 Hz (Ray *et al.* 2008*b*; Zanos *et al.* 2011) and as low as 50 Hz (Ray *et al.* 2008*a*; Ray & Maunsell, 2011) if genuine neuronal oscillations are weak or absent. Furthermore, spike contamination of electrocorticograms (ECoG) might be possible (Ray *et al.* 2008*a*).

Such findings obviously do not exclude the existence of genuine non-spiking synaptic oscillations but they do necessitate a systematic assessment of the extent of spike contamination aiming at validation of LFP analysis for the individual dataset under investigation.

We first introduce an alternative, simple method for scaling spectrograms which allows for an optimal visual inspection of amplitude/power modulation over time. This method clearly reveals the effects of spikes on LFP power. We then provide a systematic guide as to which frequencies of LFPs are contaminated by spiking activity. This guide is based on simple and realistic simulations in which we systematically investigated four parameters characterizing broadband electrophysiological signals with spiking activity: spike rate, signal-to-noise ratio (spike amplitude), spike duration and noise statistic ($1/f^{\alpha}$). These parameters can be estimated from a given dataset, and guidance about safe, non-contaminated LFP frequencies can be inferred from our results or automatically determined by a freely available script which we provide.

Methods

Ethical approval

All experimental procedures were approved by the UCL Institute of Neurology Ethical Review Procedures committee and carried out in accordance with the UK Animals (Scientific Procedures) Act.

Cortical recordings

Spikes were recorded from cortical motor areas of one awake purpose-bred macaque monkey, which was prepared for recording using deep general inhalational anaesthesia (isoflurane 1.5–2% in oxygen). Full aseptic procedures were used throughout and a full course of post-operative analgesics was given.

Spectrogram – reveal amplitude modulations

LFP amplitude modulations over different conditions or time are represented as spectrograms (colour-coded) or spectra (line plots). Due to the $1/f^{\alpha}$, $\alpha > 0$, decay of amplitude with increasing frequency, modulations in the raw presentation are dominated by lower frequencies, i.e. modulations in higher frequencies are too small to be visible. This problem is partly overcome by normalising the spectra/spectrogram: for each frequency bin separately, all amplitude values are divided by the amplitude of a defined baseline. While this can improve the presentation, modulations in higher frequencies are still prone to be overlooked. In addition, the normalisation depends strongly on the validity of the baseline. We propose the following method to overcome these deficiencies and, thereby, equally reveal modulations across all frequency bins in the highest possible detail:

$$a'_{t,f} = \frac{a_{t,f} - \min(\mathbf{a}_{:,f})}{\max(\mathbf{a}_{:,f}) - \min(\mathbf{a}_{:,f})}$$

where $a_{t,f}$ is the raw amplitude at time t for the frequency bin f and $\boldsymbol{a}_{:,f}$ is a vector of raw amplitudes across time for the frequency bin f. To avoid influence of outliers or extreme signal fluctuations on estimates of *min* and

max, normalisation can be computed based on a certain percentile range of the corresponding frequency bin, for example the 1st to 99th percentile. Depending on the data, this range can be asymmetric but should be sufficiently wide (e.g. coverage of at least 95% of all values or ± 2 standard deviations) for an optimal presentation.

Simulations

The strength of spike contamination was investigated by comparing the spectrum of pink noise with the spectrum of the same noise after real spikes had been added.

Pink noise. Noise was generated using an inverse Fourier transformation with coefficients for each frequency determined by $1/f^{\alpha}$, $0.8 \leq \alpha \leq 2$ (Little *et al.* 2007). Simulations were performed for the following noise statistics: $\alpha = 0.8$, 1, 1.2, 1.4, 1.6, 1.8 and 2.

Poisson process with refractory period. Sequences of delta pulses ranging from 1 to 150 pulses s^{-1} were created using a Poisson-like process with a refractory period of 1.5 ms and a temporal precision of 25 kHz. Pulses were created for a period of 1.31 s and then replaced using real spikes with the trough aligned to the pulse. Although neurons rarely fire at 150 spikes s^{-1} for such a long period as 1.31 s, we have chosen these parameters (a) for a high frequency resolution of 0.763 Hz in the frequency decomposition and (b) to also approximate multi-unit activity – for example four neurons producing 30 spikes s^{-1} correspond roughly to one neuron firing 120 spikes s^{-1}.

Spike recordings. Spikes were extracted from real neuronal signals sampled at 25 kHz using movable platinum–iridium microelectrodes (Thomas Recording GmbH, Giessen, Germany; tip impedance 1–2 MΩ) from primary motor (M1) and premotor (area F5) neocortex in one awake purpose-bred macaque monkey trained to grasp or observe the grasp of different objects. Details about the experimental paradigm and setup have been described previously (Vigneswaran *et al.* 2013; monkey M47).

Spikes recorded from 35 neurons in different sessions were discriminated using modified Wave_clus software (Quiroga *et al.* 2004) and extracted from the high-pass filtered signals (300 Hz acausal butterworth, 3th order) using a window of 1.36 ms (35 samples) around the spike's trough (Fig. 1*A*). The number of spikes in each of the 35 resulting spike pools was on average 2854 (range 271–8173). Average spike waveforms were added to the pink noise according to the Poisson process.

The 1.36 ms window around a spike's trough was chosen to cover all major characteristics of the spike waveform. The high-pass filter used was chosen to prevent adding potential genuine non-spike oscillations to the noise along with the average spike. The filter attenuates signals below 100 Hz by a factor smaller than 0.04. This attenuation is sufficient to reduce the strength of all signals <100 Hz below detection threshold; for example, a genuine spike-locked 10 Hz oscillation of more than 90 mV would be required to be detected in the noise. Neuronal oscillations of this strength are unlikely.

Although in this study we did not want to add any genuine spike-locked oscillations, we had to recognise that the spike itself contains genuine neuronal components below 300 Hz, which are attenuated by the filter and thereby excluded from the analysis. Applying a 300 Hz high-pass filter before adding spikes thus results in a safe but possibly incomplete estimation of spike contamination. For comparison, we performed additional simulations with average spike waveforms obtained from 0.5 Hz high-pass filtered signals. We also tested rectangular (1.36 ms) or delta pulses instead of real spike waveforms.

Signal to noise ratio (SNR). The spike amplitude for each of the 35 neurons was calculated as the peak-to-peak (peak-to-trough, min-to-max) amplitude of the corresponding average spike waveform. The noise was quantified as the root-mean-square (rms) of the spike-free pink noise. The SNR was defined as:

$$\text{SNR} = \text{average spike amplitude}/\text{rms (noise)}$$

The root-mean-square was used as an estimator of the average noise power and is identical to the standard deviation if the mean is zero. The resulting SNR is thus directly comparable to other SNR definitions (Fig. 1*B*); for example, the SNR used here is two times that used by Suner *et al.* (2005) and Jackson & Fetz (2007). Spike amplitudes were assumed to reach maximal values around 1 mV with SNRs up to 30 (experience in this laboratory and, for example, Jackson & Fetz, 2007). Simulations were performed for the following SNRs: 0 (control), 1, 1.5, 2, 2.5, 3, 3.5, 4, 5, 6, 7, 8, 9, 10, 12, 14, 16, 18, 20, 25 and 30.

Frequency analysis. A Blackman–Harris taper was applied to the 1.31 s (exact value: 2^{15} samples at 25 kHz) of noise or noise plus spikes before Fourier transformation (Matlab 2012*b*, blackmanharris and fft). These parameters were chosen for high frequency resolution (0.763 Hz) and reduced bias and variability in the spectra/spectrograms. Note that this window length does not mean that spike trains have to occur for a period of 1.31 s for the presented results to be correct. For spike contamination to occur around 10 Hz, the duration of a spike train can be much

shorter than 100 ms, a period which is not unrealistic (see, for example, Fig. 3*A*). Contaminations in higher frequencies can occur for even shorter spike trains; for example, for contamination around 100 Hz the duration of a spike train can be shorter than 10 ms.

The same parameters were used for estimation of the frequency composition of the spike waveforms, whereas the 1.31 s window was padded with zeroes outside the waveform.

Statistical tests. For each neuron, spike rate, SNR and noise statistic ($1/f^{\alpha}$), 100 datasets of noise and the identical noise plus spikes were created. Amplitudes for each frequency bin were computed for both conditions: noise without spikes and noise with spikes. These 100 amplitude values per condition were tested for significant differences using Wilcoxon's signed-rank test. Resulting *P*-values were corrected for multiple testing using false-discovery rate (FDR) correction (Benjamini & Hochberg, 1995) with $P < 0.05$ for each spike rate/SNR dataset, i.e. separately for each neuron and noise statistic.

Determination of risk zone boundaries. For each neuron, SNR and noise statistic, the corrected *P*-values were arranged in a plane with axes 'spike rate' and 'frequency'. In these planes, critical boundaries separating regions of non-significant (towards low spike rates and frequencies) from significant (towards high spike rates and frequencies) spike contamination were determined as follows. First, we searched in each frequency bin for transitions from non-significant to significant neighbouring *P*-values along the 'spike rate' axis. The smaller spike rate of each transition was saved as *x*-coordinate and the frequency bin as *y*-coordinate. A curve was fitted to these coordinates using a two-dimensional robust linear fit (Matlab 2012*b*, smooth with parameters 0.1 and 'rlowess'). Finally, the fitted curve was shifted by 3 Hz (−92 dB highest sidelobe peak, Blackman–Harris, window length 2^{15} at 25 kHz) towards higher frequencies to compensate for any bias in the frequency analysis and to obtain a conservative boundary.

Results

Dynamic spectrograms

We introduced here an alternative method to rescale spectrograms. The method reveals amplitude modulations equally across all frequencies and is independent of the choice of baseline level. To illustrate this method we applied it to the LFP recorded in primary motor cortex of an awake, behaving macaque monkey performing a

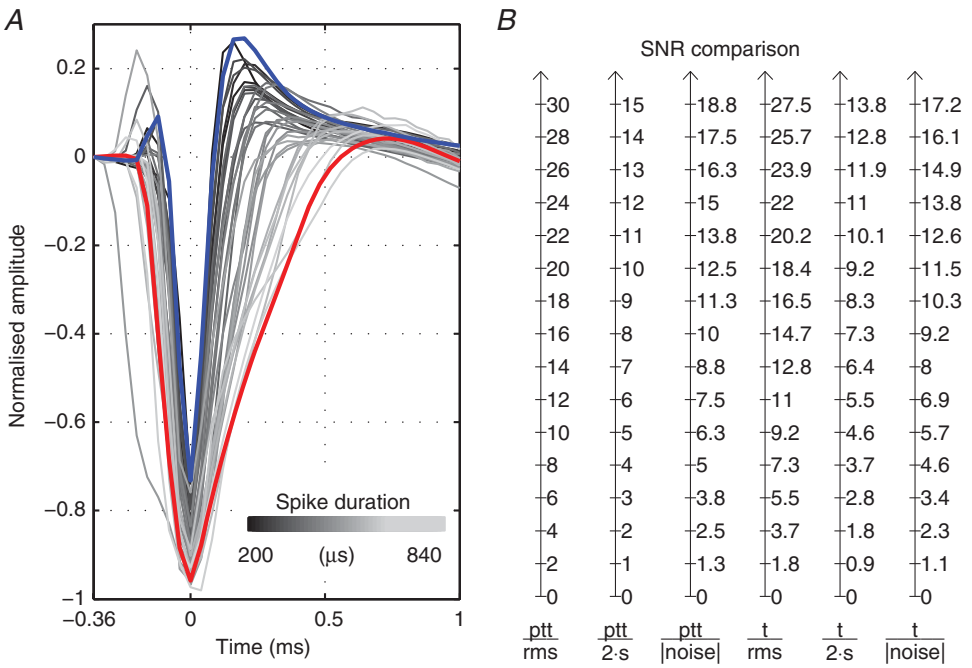

Figure 1. Average spike waveforms and SNR comparison
A, normalised average spike waveforms (extracted from 300 Hz high-pass filtered signal) for all 35 neurons used in the simulations and the 1.36 ms window used to extract the part of the spikes which was added to the pink noise. Neurons with blue and red waveform were used in Figs 6 and 9. Brightness of waveform reflects spike duration: dark, short spike duration; bright grey, long spike duration. *B*, comparison of different measures for the SNR (spike amplitude: ptt, peak to trough; t, trough; RMS, root mean square; 2 · std, 2 times standard deviation; |noise|, amplitude 5th to 95th percentiles; first measure used in this study).

grasping task (Vigneswaran *et al.* 2013). Figure 2*A* shows the raw amplitude spectrum (computed as described in the Methods) averaged over multiple trials and aligned to movement onset at time zero. Due to the $1/f^{\alpha}$ property of the spectrum, the low frequencies (<10 Hz) clearly dominate the plot and conceal amplitude modulations at higher frequencies. Well-known phenomena such as a power increase in gamma range and drop in beta range (~20 Hz) accompanying movements (Pfurtscheller, 1989; Arroyo *et al.* 1993) are hardly apparent in this type of presentation. Different techniques were introduced to overcome this problem. One of the most common is normalisation of the amplitude spectrum to a predefined baseline activity (Fig. 2*B*). In addition, one can also take a logarithm of the baseline-normalised spectrum and present the results in decibels (Fig. 2*C*). Although these methods clearly improve presentation of the data, they significantly depend on the choice of the baseline period. Furthermore, amplitude modulations at some frequencies can still overshadow smaller but significant changes at other frequencies.

We normalised the amplitude spectrum for each frequency bin to the minimum and maximum amplitude for this frequency bin in the presented time window (here −3.34 s to 3.34 s, see Methods for details). Our method considers all frequencies independently and utilises the full *dynamical* false-colour range for presentation of each frequency bin (Fig. 2*D*). *Dynamical spectrograms* are also independent of a baseline choice.

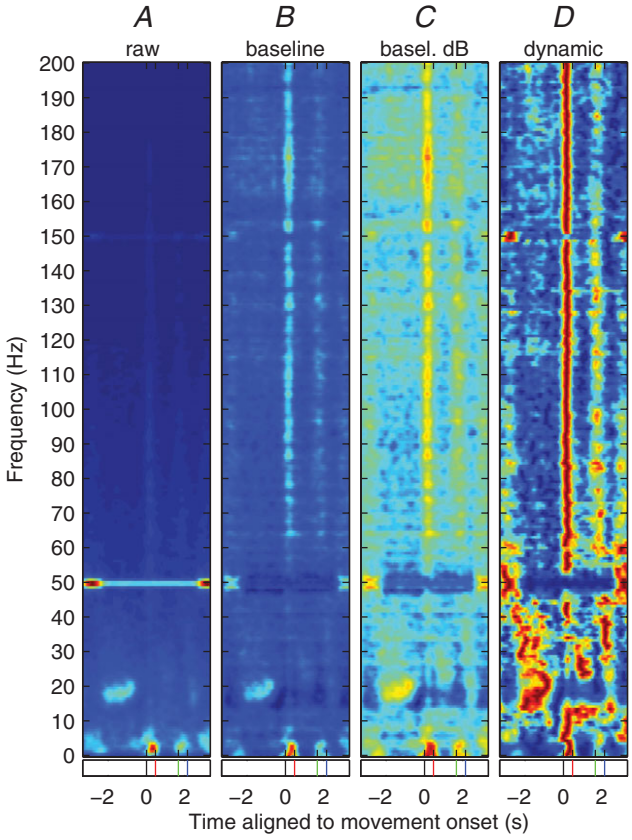

Figure 2. 'Dynamical' normalisation compared to other types of spectrograms
Spectrograms for the same intra-cortical LFP recorded in macaque monkey primary motor cortex. The monkey started movement at time = 0 s and grasped, pulled and held (red dash) an object before releasing (green dash) the object and returning to a home pad (blue dash). The time window comprises −3.34 to +3.34 s around movement onset ($t = 0$ s). *A*, raw spectrogram; *B*, normalised to a baseline (mean over first three time steps at the beginning of the time window); *C*, first normalised to a baseline as in *B*, then converted to decibels; and *D*, 'dynamic spectrogram' obtained using the method proposed here.

Influence of spiking activity on LFPs

We applied the proposed method 'dynamic spectrogram' to the intra-cortical broadband signal, which includes both LFP and spiking activity, as shown in Fig. 3*A*. The dynamic spectrogram clearly reveals an increase in amplitude during the period of spiking activity (0.5–1.5 s) up to the Nyquist frequency (12.5 kHz; Fig. 3*B*) and, even more relevant for this study, also for frequencies below 150 Hz. Is this increase caused by spiking activity in the recording or does it represent genuine changes in brain oscillatory activity? To answer this question, we performed extensive realistic simulations by artificially adding real spike shapes to the background activity and varying (1) the amplitude of spikes relative to the background activity (SNR), (2) spike rate, (3) spike duration (by using 35 different neurons) and (4) background activity statistics (α of $1/f^{\alpha}$ spectrum).

Figure 4*A* (top left subplot) visualises an excerpt of pink noise (SNR 0, $1/f^{1.4}$) and (other small subplots) the identical noise with a sample spike train generated according to a Poisson-like spiking process with a refractory period (see Methods) and scaled according to the SNR indicated on the plot. Figure 4*A* (centre) shows the colour-coded ratio of the amplitude spectra of pink noise with added spikes to the spectra of the same pink noise without spikes. It summarises the changes across frequencies, SNR and a range of realistic firing rates. With increasing spike rate and SNR, the degree of spike contamination increased and affected more and more frequencies, including lower frequencies. Starting at low firing rates and SNRs, an increase in amplitude was first observed for frequencies between around 500 and 3000 Hz, frequencies commonly included in investigations of spiking activity. The affected frequency range then became wider with higher spike rates and SNRs, eventually contaminating frequencies below 150 Hz. To illustrate the spectral changes with increase in firing rate (Fig. 4*B*) we calculated a raw spectrum for constant SNR and noise statistic (5, $1/f^{1.4}$). Even low spike rates (~30 spikes s^{-1})

caused non-uniform, waveform-dependent amplitude increases across a wide range of frequencies, and were apparent in spectrograms for activity with frequencies as low as 25 Hz (Fig. 4*B*).

To estimate what level of spike contamination leads to spurious results, i.e. false conclusions about significant changes in LFP due to genuine oscillatory activity, we statistically compared (Wilcoxon's signed-rank test) 100 simulations of pink noise *versus* the same pink noise (per simulation) but with spikes added. The test returned *P* values for each spike rate, SNR and noise statistic (Fig. 5, example). All *P* values were corrected for FDR of multiple testing (see Methods). In addition to this correction, the finding that significant (grey shades) and not significant (white) *P* values are not randomly distributed but instead form contiguous regions (clusters) speaks against this result being due to false positives (Type I errors) and corroborates the interpretation of which LFP frequencies are contaminated. The boundaries (Fig. 5, red line) separating the region of non-significant from significant spike-related amplitude increases (spike contamination) were determined automatically (see Methods).

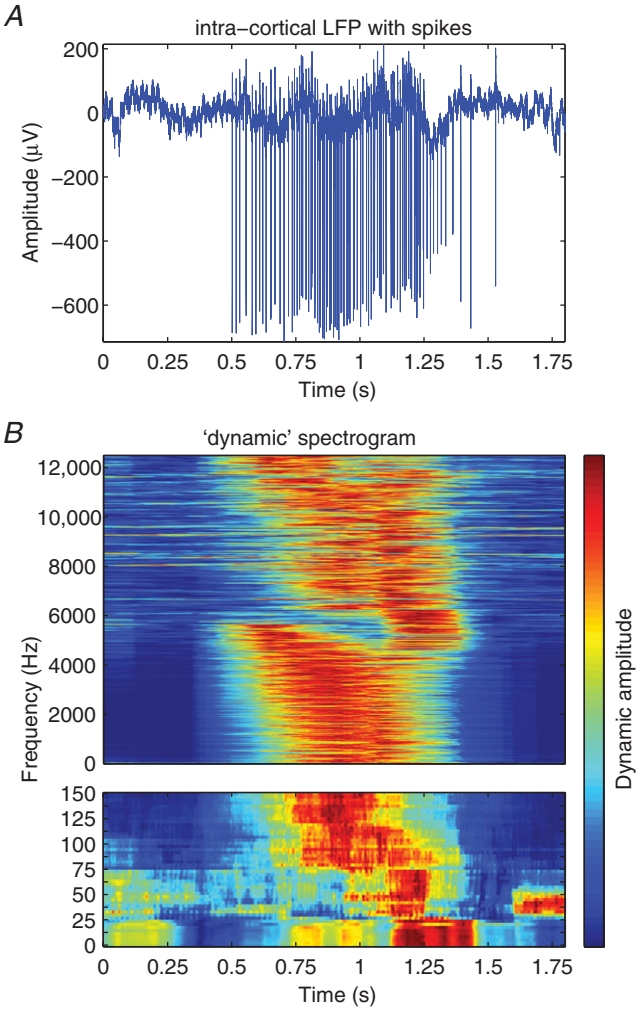

Figure 3. Real intra-cortical signal and corresponding 'dynamic' spectrogram
A, a real intra-cortical signal with spiking activity recorded in monkey primary motor cortex during a reach and grasp task. *B*, spectrograms calculated using the 'dynamic spectrogram' method.

Using these boundaries, we could confirm that spikes already significantly affect frequencies below the often-used 300 Hz threshold (Fig. 6). While the neuron presented in Fig. 6*A* (blue waveform in inset and Fig. 1*A*) shows less severe contamination, the neuron presented in Fig. 6*B* (red waveform in inset and Fig. 1*A*) shows how readily spike contamination of LFP can occur even for low SNRs and spike rates (e.g. SNR 2 and 30 spikes s^{-1}). Moreover, we found that spikes significantly affected frequencies below 100 Hz for realistic values of SNRs (7–16) and spike rates (<100 spikes s^{-1}). Even more importantly, these results indicate that spikes can contaminate neuronal oscillations down to around 10 Hz (using pink noise as surrogate for cortical, electrophysiological 'noise').

While Fig. 6 shows the extent of spike contamination for just two examples of different single neurons, neuronal recordings can contain the spiking activity of multiple neurons. When multiple neurons fire (independently), their spike rates roughly add up and boost spike contamination; for example, three neurons each spiking with 20 spikes s^{-1} and equal SNR would correspond to one neuron spiking with 60 spikes s^{-1}. Although only results obtained from single-unit activity are presented, spike contamination for multi-unit activity can thus be inferred from Fig. 6 and the following figures.

The results so far were based on a pink noise with a constant $\alpha = 1.4$ ($1/f^{1.4}$), an average value we found in our recordings. As the noise parameters might differ between different brain areas or recording conditions, we simulated noise with other plausible α and found that it substantially affects the strength of spike contamination (Fig. 7). This is especially apparent for spikes with low SNRs: while there was no contamination in frequencies below 300 Hz for small α (e.g. $1/f^{0.8}$, curves for SNR <2 not present), spikes with an SNR as low as 1 contaminated frequencies down to around 65 Hz for large α ($1/f^{2}$, top curve SNR = 1). The effect of noise was much weaker for higher SNRs.

While the previous results were obtained for individual neurons, Fig. 8 shows the median (continuous lines) and maximal contamination (dashed lines) across 35 arbitrary neurons (Fig. 1) for typical SNRs. As the spike amplitude was normalised in terms of SNR before calculations were carried out, the variability in strength of contamination across neurons must have originated from differences in the spike waveforms. Frequency analysis of the waveforms (see Methods) revealed that broad spikes have stronger components in frequencies below ~1 kHz than short spikes (Fig. 9*A*). This result also explains the stronger

contamination of the wide-spike neuron (peak to trough: 0.76 ms) as compared to the short-spike neuron (peak to trough: 0.24 ms) as presented in Fig. 6*B* and 6*A*, respectively.

One parameter directly characterising the spike waveform is spike duration. Consistent with the frequency composition of corresponding waveforms (Fig. 9*A*), we found that the strength of contamination depends substantially on the spike duration; the wider the spike (peak to trough) the larger the extent of spike contamination (Fig. 9*B*). The neuronal data contributing to Fig. 6 are representative of narrow spike neurons (brief waveforms, weak contamination) and of wide spike neurons (long spike duration, strong contamination, cf. insets and Fig. 1*A*). If neurons fire even broader spikes, contamination can potentially be stronger than shown in Fig. 6*B*; however, contamination strength seems to plateau at these broad spike durations (Fig. 9*B*).

The dependency between spike duration and strength of contamination was significant ($P < 0.05$, FDR corrected) for all spike rates above 2–3 spikes s^{-1} and SNRs above 7. For lower SNRs the spike rate had to be higher to be significant (Fig. 9*C*).

The results presented so far were based on spike waveforms obtained by averaging real spikes from 300 Hz high-pass filtered intra-cortical recordings (see Methods). This precaution was taken to prevent adding potential genuine spike-locked oscillatory activity in low frequencies along with the average spike waveform to the pink noise. This procedure might also remove signal components

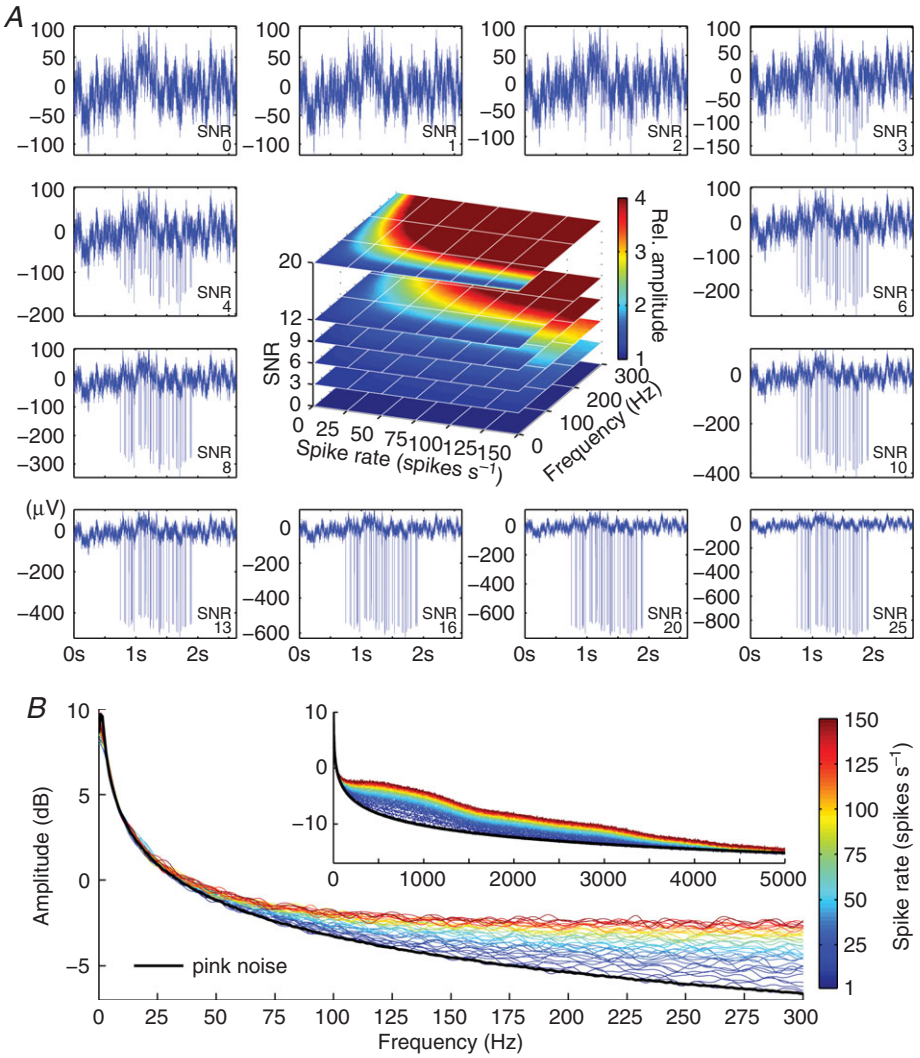

Figure 4. SNRs and spike spectra
A, outer insets: identical pink noise ($1/f^{1.4}$) and spike train with spike amplitudes scaled according to exemplary SNRs as indicated; central inset: typical spectra with colour-coded relative amplitudes (amplitudes of noise with spikes *vs.* noise alone). Limits of colour bar are set to 1 (minimum) to 4 for presentation purposes; the real upper limit was higher, especially for high SNRs. *B*, amplitude spectra (dB) for different spike rates but fixed SNR = 5 and noise statistic $1/f^{1.4}$.

of the spikes below 300 Hz and result in an incomplete estimate of spike contamination. However, using a 0.5 Hz high-pass filter before averaging the spikes resulted qualitatively in the same results. The script provided along with this study (http://www.carmen.org.uk/portal) automatically estimates the extent of spike contamination for both filter cutoffs.

In our simulation using real spikes, contamination was (1) for almost all neurons larger than using a delta pulse as an approximation of a spike and (2) for all neurons smaller than using a rectangular 1.36 ms pulse as another approximation (Fig. 9*B*). This emphasises the necessity of using real spike waveforms in estimations of the extent of spike contamination in LFP recordings.

Discussion

We have introduced an alternative method to rescale spectrograms, investigated the contamination of LFP by spikes and provided a guide to the contribution of spikes to recorded LFP activity.

Dynamic spectrogram

The 'dynamic spectrogram' method reveals amplitude modulations equally across all frequencies. It is independent of any baseline and allows for visual presentation of the spectrogram in great detail. The method can be applied to any type of recording (LFP/ECoG/electroencephalography (EEG)/magentoencephalography (MEG)) to reveal amplitude modulations, which may otherwise remain undetected. In contrast to commonly used methods such as normalisation or log-normalisation, this method overcomes common problems in the presentation of spectrograms. First, higher amplitudes and amplitude modulations at low frequencies do not mask modulations at higher frequencies. Secondly, the method is robust to artefacts as only the frequency bins containing the artefact are affected and the percentile range on which the minimum and maximum is calculated can be adapted to the dataset analysed. Thirdly, as it is baseline independent, it is not necessary to search for an optimal baseline and ongoing brain activity or artefacts during a baseline period do not affect analysis of other task phases.

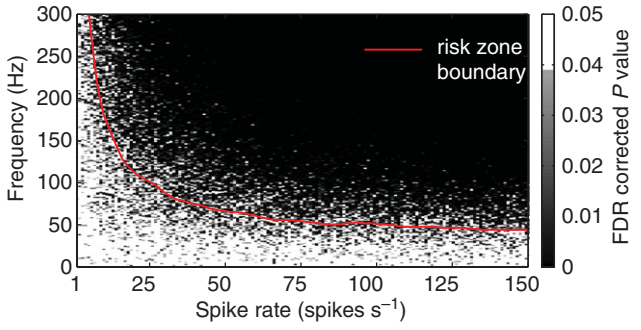

Figure 5. Example of boundary separating zones of significant *versus* non-significant spike contamination
FDR-corrected *P* values in grey shades as returned by Wilcoxon's signed-rank test for 100 runs of noise *versus* noise plus spikes. The boundary was determined automatically using robust linear fitting of the transition between both zones and shifted upwards by 3 Hz to compensate for bias in frequency decomposition (see Methods).

The proposal to use this method for displaying (dynamic) spectrograms should not be misinterpreted as questioning the validity of normalising spectrograms to a baseline period. If a neurophysiologically justified and artefact-free baseline can be defined, baseline normalisation is a different but valid approach. Dependent on study objectives and careful statistics, frequency bins can also be separately normalised by individually selecting appropriate baseline values from a pre-defined, pre-stimulus time window (e.g. Waterstraat *et al.* 2012). However, 'dynamic spectrograms' guarantee that the full false-colour space is used for every individual frequency bin, which is essential to equally reveal and present modulations in high detail across all frequency bins.

These optimizations are achieved by sacrificing a direct quantitative comparison across frequencies or different experimental conditions, which can still be carried out using rigorous analysis.

Spike contamination

Using simple and realistic simulations, we showed that, first, spikes can contaminate LFPs in frequencies below 300 Hz, which is in line with previous studies reporting contamination down to 100 Hz (Quilichini *et al.* 2010; Ray & Maunsell, 2011; Belluscio *et al.* 2012; Schomburg *et al.* 2012). Moreover, we (1) systematically investigated spike contamination and (2) demonstrated how easily frequencies <100 Hz, often considered to be 'safe', can be affected in realistic recordings and that contamination can even occur down to around 10 Hz.

As the spike waveform itself already contains frequencies down to 100 Hz (Fig. 9*A*, cf. Zanos *et al.* 2012), it is evident that even a few spikes can significantly contaminate the LFP. However, another factor is the presence of spike trains effectively resulting in an amplitude increase in a broad, contiguous range of frequencies. The pattern of this increase (Fig. 4*B*) depends on the spike waveform. Neurons firing broader spikes contaminate the LFP to a greater extent because their waveforms have stronger components in lower frequencies than short spikes (Fig. 9).

Pacemaker neurons that fire coupled to a certain rhythm and spike synchrony can increase the extent of spike contamination. The boundaries suggested in this study would then have to be shifted further down in frequency.

A similar effect can occur for uncorrelated multi-unit spiking activity as here spikes can temporally overlap, which effectively increases the SNR. However, even for higher spike rates such incidents are relatively rare due to the brevity of individual spikes.

Consequences of spike contamination

We showed that even a simple analysis in the frequency domain can be affected by spike contamination. The same arguments hold for other analyses in the frequency domain, e.g. spike–LFP coherence. Any analysis in the time domain is even more prone to spike contamination because it requires spike removal from the data, and low-pass filtering is not sufficient to achieve this. As the amplitude of spikes can be orders of magnitudes larger than that of LFPs (e.g. up to 1 mV *vs.* a few microvolts), higher spike-related frequencies remain after filtering. For example, a 200 Hz (450/1000) signal fluctuation of 100 μV (10/1) would remain if a third-order 100 Hz low-pass Butterworth filter was applied to a signal containing spikes with an amplitude of 1 mV (for the aforementioned frequencies). The spike-triggered average of LFPs is even more prone to this misinterpretation since after averaging the amplitude of the spike is maintained but the noise level scales down with the square-root of the number of spikes used for averaging (assumption: Gaussian noise). Even very low-amplitude filter residuals in frequencies above the low-pass filter cut-off can emerge.

Furthermore, a single spike also contains very low frequencies. Although low in amplitude, these frequencies can emerge if the noise is reduced sufficiently by averaging the LFP with reference to a large number of spikes. The spike-triggered LFP must be generated using unfiltered data recorded with an as high as possible sampling rate and only filtered after the spike had been removed.

By contrast, interaction between spikes and neuronal oscillations (Buzsaki *et al.* 2012), either by genuine electrophysiological processes or by spike contamination, can have useful applications. Even if reliable spiking activity cannot be recorded, LFPs can reflect their activity and therefore be used as a BMI control signal for example. Furthermore, the LFP is partly predictable from spiking activity (David *et al.* 2010) and vice versa (Hall *et al.* 2012).

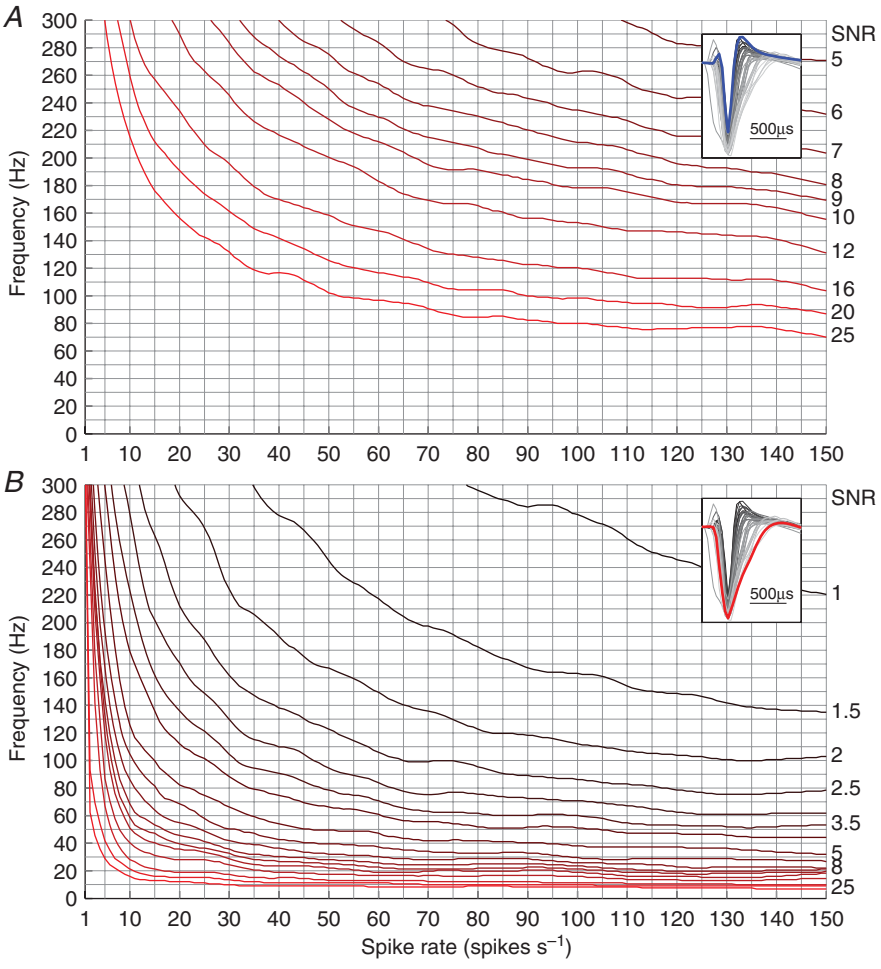

Figure 6. Spike contamination for different SNRs and two typical neurons
Frequencies above each curve are significantly affected by spike contamination. For clarity, only sample SNRs are shown and labelled. Increasing SNRs consistently caused contamination in progressively lower frequencies. Representative neurons exhibiting weak spike contamination (*A*, Fig. 1 blue curve and inset), and strong spike contamination (*B*, Fig. 1 red curve and inset).

Hence, our results have direct implications for the stability of LFP recordings and usefulness of the LFP as a control signal for BMIs. Changes in spiking activity can substantially alter the LFP down to 10 Hz and thus change the BMI input signal. Stable recordings of LFP would in certain situations be comparable to those of identified neurons (Dickey *et al.* 2009; Fraser & Schwartz, 2012).

However, LFPs in frequencies below ∼7 Hz do carry substantial information about movement parameters (Waldert *et al.* 2009). A better long-term stability might thus be expected for low-frequency BMIs.

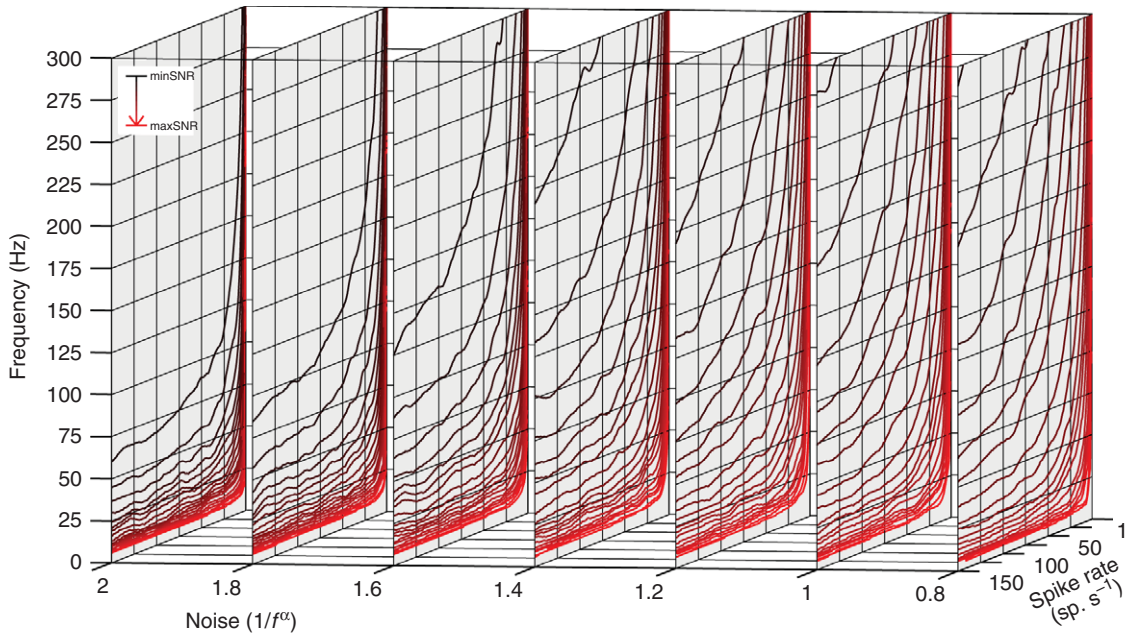

Figure 7. Influence of noise statistic on spike contamination
Each vertical plane shows spike contamination for different SNRs as in Fig. 6 (high/low SNRs in black/red, i.e. SNRs increase from top to bottom) as a function of the noise statistic ($1/f^{\alpha}$). Same neuron as in Fig. 6*B*, i.e. red curve Figs 1*A* and 9*A* and red symbols in Fig. 9*B*.

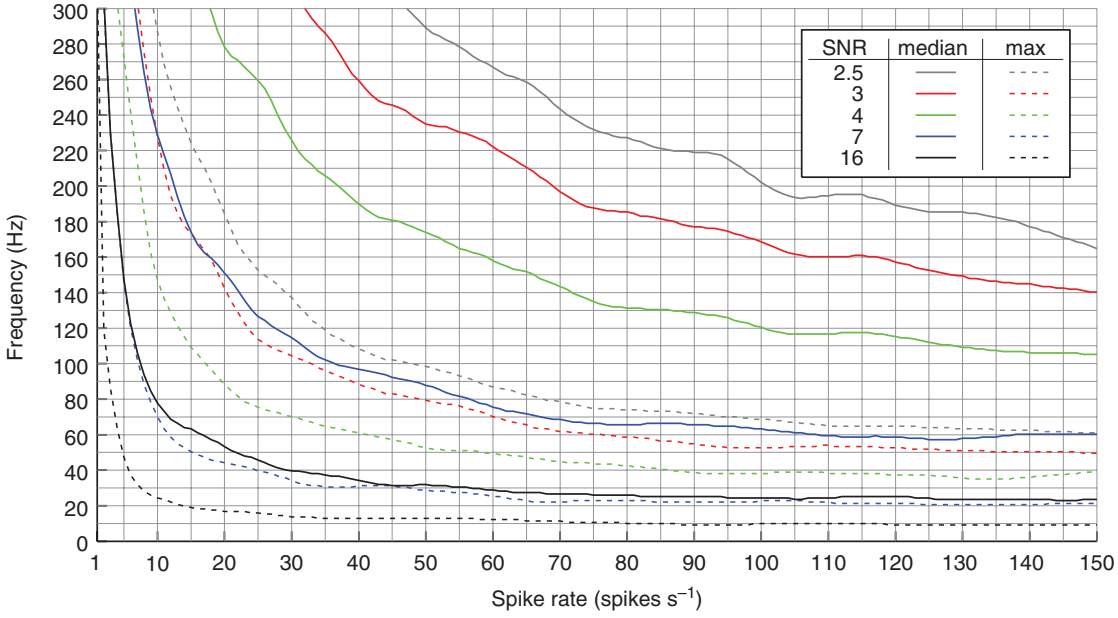

Figure 8. Overall spike contamination
Median and maximal spike contamination across 35 neurons for typical SNRs.

Can spike contamination be prevented?

If the signal was recorded with broad filters, i.e. it is possible to identify spikes in the recordings, spike removal algorithms can be used to mitigate spike contamination (Galindo-Leon & Liu, 2010; Zanos *et al.* 2011). Replacing spike samples with interpolated values (Oostenveld *et al.* 2011), a mean value or noise, for example, can ameliorate contamination mainly of low LFP frequencies in case of high-amplitude, detectable spikes, i.e. high SNRs. However, even though spike contamination is gradually weakened with every spike removed, it can only be completely prevented if all action potentials, including those which cannot be separated into activity of single neurons, are removed. To this end, algorithms would have to be tuned to detect low-amplitude spikes as well, whereas standard ones are optimised to identify relatively large spikes rather than all spiking activity. Low-amplitude spikes can remain undetected and, as this study has shown, contaminate LFPs (e.g. Fig. 7, $\alpha = 2$: below 75 Hz (high-gamma), SNR = 1 (top curve) or below 50 Hz, SNR = 1.5). Contamination is even more severe for noise with an $\alpha > 2$ or for multi-unit spiking activity, which can temporally produce spike rates far above 150 spikes s^{-1} if multiple neurons coincidentally fire spikes or spike bursts around the same time.

Even more importantly, if the LFP signal was low-pass filtered before recording, spike removal techniques cannot be applied and hence spike contamination cannot be prevented. Low-pass filter in the recording system must thus be chosen as high as possible (>2 kHz). Other factors might include whether brain tissue has low-pass filtering properties (Nunez & Srinivasan, 2006; Logothetis *et al.* 2007) and whether low-impedance electrodes may still record low-frequency components of spiking activity contaminating the LFP. In all cases high-frequency components necessary for spike detection (and subsequent spike removal) would not be available and spike contamination of the LFP unavoidable, even in the case of originally higher SNRs.

One indicator for the presence of spike contamination or spikes, even if concealed by low-pass filtering, is an amplitude increase in wide continuous frequency bands as revealed with the proposed 'dynamic spectrogram' (Fig. 2).

Genuine neuronal oscillations despite spikes

Our concern over possible contamination of LFP with spiking activity should not be interpreted as undermining the importance of genuine oscillations in LFP activity. In many realistic scenarios, LFP frequencies up to the high-gamma band do reflect genuine neuronal oscillations despite the presence of spikes in the recorded data. This statement is based, first, for example on observations of neuronal oscillations in these frequency ranges showing anti-correlated changes in spiking activity and amplitudes of oscillations (Ray & Maunsell, 2011). Secondly, high-gamma oscillations are observed in ECoG, EEG and MEG, techniques providing signals of lower spatial resolution and information content than LFP (Waldert *et al.* 2009). While there are models showing that synchronous spikes could potentially generate currents detectable with ECoG (Ray *et al.* 2008a), ECoG is thought to be dominated by extra-dendritic currents and not spikes. EEG and MEG, characterized by an even larger source–sensor distance and thus unlikely to be affected by

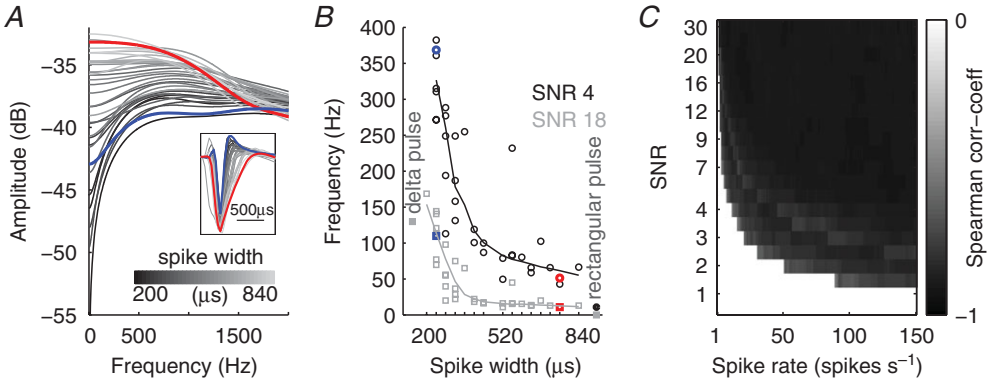

Figure 9. Effect of spike duration on strength of contamination
A, frequency composition below 2 kHz of the different, normalised spike waveforms (inset). *B*, spike duration of each neuron (empty symbols) and the corresponding frequency above which the LFP is significantly contaminated (two typical SNRs and fitted curves, blue and red symbols correspond to neurons in Figs 1*A*, 6 and 9*A*). For comparison, the values for using delta and rectangular pulses (filled symbols) instead of real spikes are shown. Contamination was always stronger for rectangular pulses. Using delta pulses results in an underestimation of spike contamination. *C*, Spearman correlation between spike duration and strength of contamination for all SNRs (only significant ($P < 0.05$, FDR-corrected) correlation coefficients are shown, scaled from 0 to −1 because no positive correlation is present).

spikes, reflect neuronal oscillations in high frequencies (Gonzalez *et al.* 2006; Cheyne *et al.* 2008). Electrical stimulation of the median nerve was reported to elicit MEG oscillations as high as 600 Hz (Haueisen *et al.* 2001; Waterstraat *et al.* 2012). A maximum possible frequency of neuronal oscillations has not yet been deduced.

However, note also that EEG/MEG above 20 Hz is prone to a contamination by electromyography (EMG) (Whitham *et al.* 2007). Indicators for genuine neuronal oscillations instead of spike (LFP) or EMG (EEG/MEG) contamination can be amplitude increases in distinctive rather than contiguous frequency bands, as revealed by the proposed 'dynamic spectrogram', or uncorrelated changes in spiking activity and amplitudes of oscillations.

Assessment of spike contamination

This study demonstrated the difficulty in excluding spiking activity from LFP analysis, even if detectable spikes were removed. Applying frequency cut-offs through low-pass filters or any frequency-based analyses can be sufficient in some situations but must be chosen carefully, i.e. either very low or individually adjusted to the dataset. The systematic, straightforward guide provided through Figs 6–9 helps to estimate the extent of spike contamination and thus to choose the cut-off for the data under investigation.

To further support the assessment of spike contamination, we provide a script which analyses the data the researcher is interested in and returns the boundary. This script is easy to use as it requires as input only the data to be analysed. It then returns for every time point the estimated frequency above which the LFP is contaminated by spikes. However, this script can only provide an estimate for periods with detectable spikes. The LFP above ∼100 Hz should always be investigated with great care. Even if no spikes are detectable, low-amplitude spikes (SNR = 1–1.5) might be present and contaminate the LFP. Spike removal techniques cannot overcome this problem.

Conclusions

Spikes can generate significant signal changes that appear as neuronal oscillations in almost all commonly investigated frequency bands: alpha/mu, beta, gamma and high-gamma. In signals below 10 Hz, such as the movement-related potential, delta or theta bands, spike contamination is theoretically possible but unrealistic. The extent of spike contamination is strongly influenced by noise, spike amplitude, rate and duration. It is crucial to assess spike contamination for each individual dataset; simply applying a frequency threshold or spike removal cannot fully prevent such contamination. The present study helps to identify spike contamination and provides a systematic, straightforward guide (findings and script) to assessment of spike contamination in intra-cortical LFPs.

References

Arroyo S, Lesser RP, Gordon B, Uematsu S, Jackson D & Webber R (1993). Functional significance of the mu rhythm of human cortex: an electrophysiologic study with subdural electrodes. *Electroencephalogr Clin Neurophysiol* **87**, 76–87.

Bair W, Koch C, Newsome W & Britten K (1994). Power spectrum analysis of bursting cells in area MT in the behaving monkey. *J Neurosci* **14**, 2870–2892.

Belluscio MA, Mizuseki K, Schmidt R, Kempter R & Buzsaki G (2012). Cross-frequency phase–phase coupling between theta and gamma oscillations in the hippocampus. *J Neurosci* **32**, 423–435.

Benjamini Y & Hochberg Y (1995). Controlling the false discovery rate: a practical and powerful approach to multiple testing. *J Roy Statist Soc Ser B (Methodological)* **57**, 289–300.

Buzsaki G, Anastassiou CA & Koch C (2012). The origin of extracellular fields and currents–EEG, ECoG, LFP and spikes. *Nature Rev Neurosci* **13**, 407–420.

Cheyne D, Bells S, Ferrari P, Gaetz W & Bostan AC (2008). Self-paced movements induce high-frequency gamma oscillations in primary motor cortex. *Neuroimage* **42**, 332–342.

David SV, Malaval N & Shamma SA (2010). Decoupling action potential bias from cortical local field potentials. *Comput Intell Neurosci* 393019.

Dickey AS, Suminski A, Amit Y & Hatsopoulos NG (2009). Single-unit stability using chronically implanted multielectrode arrays. *J Neurophysiol* **102**, 1331–1339.

Fraser GW & Schwartz AB (2012). Recording from the same neurons chronically in motor cortex. *J Neurophysiol* **107**, 1970–1978.

Galindo-Leon EE & Liu RC (2010). Predicting stimulus-locked single unit spiking from cortical local field potentials. *J Comput Neurosci* **29**, 581–597.

Gonzalez SL, Grave de Peralta R, Thut G, Millan Jdel R, Morier P & Landis T (2006). Very high frequency oscillations (VHFO) as a predictor of movement intentions. *Neuroimage* **32**, 170–179.

Haueisen J, Schack B, Meier T, Curio G & Okada Y (2001). Multiplicity in the high-frequency signals during the short-latency somatosensory evoked cortical activity in humans. *Clin Neurophysiol* **112**, 1316–1325.

Jackson A & Fetz EE (2007). Compact movable microwire array for long-term chronic unit recording in cerebral cortex of primates. *J Neurophysiol* **98**, 3109–3118.

Hall T, Nazarpour K & Jackson A (2012). Real-time prediction and biofeedback control of individual neurons using spike-related slow potentials. 42th SfN Neuroscience Meeting, New Orleans, USA.

Little MA, McSharry PE, Roberts SJ, Costello DA & Moroz IM (2007). Exploiting nonlinear recurrence and fractal scaling properties for voice disorder detection. *Biomed Eng Online* **6**, 23.

Logothetis NK (2003). The underpinnings of the BOLD functional magnetic resonance imaging signal. *J Neurosci* **23**, 3963–3971.

Logothetis NK, Kayser C & Oeltermann A (2007). *In vivo* measurement of cortical impedance spectrum in monkeys: implications for signal propagation. *Neuron* **55**, 809–823.

Mehring C, Rickert J, Vaadia E, Cardoso de Oliveira S, Aertsen A & Rotter S (2003). Inference of hand movements from local field potentials in monkey motor cortex. *Nature Neurosci* **6**, 1253–1254.

Nunez PL & Srinivasan R (2006). *Electric Fields of the Brain*, 2nd ed. Oxford University Press, Oxford.

Oostenveld R, Fries P, Maris E & Schoffelen JM (2011). FieldTrip: Open source software for advanced analysis of MEG, EEG, and invasive electrophysiological data. *Comput Intell Neurosci* **2011**, 156869.

Pfurtscheller G (1989). Functional topography during sensorimotor activation studied with event-related desynchronization mapping. *J Clin Neurophysiol* **6**, 75–84.

Quilichini P, Sirota A & Buzsaki G (2010). Intrinsic circuit organization and theta-gamma oscillation dynamics in the entorhinal cortex of the rat. *J Neurosci* **30**, 11128–11142.

Quiroga RQ, Nadasdy Z & Ben-Shaul Y (2004). Unsupervised spike detection and sorting with wavelets and superparamagnetic clustering. *Neural Comput* **16**, 1661–1687.

Ray S, Crone NE, Niebur E, Franaszczuk PJ & Hsiao SS (2008*a*). Neural correlates of high-gamma oscillations (60–200 Hz) in macaque local field potentials and their potential implications in electrocorticography. *J Neurosci* **28**, 11526–11536.

Ray S, Hsiao SS, Crone NE, Franaszczuk PJ & Niebur E (2008*b*). Effect of stimulus intensity on the spike–local field potential relationship in the secondary somatosensory cortex. *J Neurosci* **28**, 7334–7343.

Ray S & Maunsell JH (2011). Different origins of gamma rhythm and high-gamma activity in macaque visual cortex. *PLoS Biol* **9**, e1000610.

Schalk G, Kubánek J, Miller KJ, Anderson NR, Leuthardt EC, Ojemann JG, Limbrick D, Moran D, Gerhardt LA & Wolpaw JR (2007). Decoding two-dimensional movement trajectories using electrocorticographic signals in humans. *J Neural Eng* **4**, 264–275.

Schomburg EW, Anastassiou CA, Buzsaki G & Koch C (2012). The spiking component of oscillatory extracellular potentials in the rat hippocampus. *J Neurosci* **32**, 11798–11811.

Suner S, Fellows MR, Vargas-Irwin C, Nakata GK & Donoghue JP (2005). Reliability of signals from a chronically implanted, silicon-based electrode array in non-human primate primary motor cortex. *IEEE Trans Neural Syst Rehabil Eng* **13**, 524–541.

Vigneswaran G, Philipp R, Lemon RN & Kraskov A (2013). M1 corticospinal mirror neurons and their role in movement suppression during action observation. *Curr Biol* **23**, 236–243.

Waldert S, Pistohl T, Braun C, Ball T, Aertsen A & Mehring C (2009). A review on directional information in neural signals for brain–machine interfaces. *J Physiol Paris* **103**, 244–254.

Waldert S, Preissl H, Demandt E, Braun C, Birbaumer N, Aertsen A & Mehring C (2008). Hand movement direction decoded from MEG and EEG. *J Neurosci* **28**, 1000–1008.

Waterstraat G, Telenczuk B, Burghoff M, Fedele T, Scheer HJ & Curio G (2012). Are high-frequency (600 Hz) oscillations in human somatosensory evoked potentials due to phase-resetting phenomena? *Clin Neurophysiol* **123**, 2064–2073.

Whitham EM, Pope KJ, Fitzgibbon SP, Lewis T, Clark CR, Loveless S, Broberg M, Wallace A, DeLosAngeles D, Lillie P, Hardy A, Fronsko R, Pulbrook A & Willoughby JO (2007). Scalp electrical recording during paralysis: quantitative evidence that EEG frequencies above 20 Hz are contaminated by EMG. *Clin Neurophysiol* **118**, 1877–1888.

Zanos S, Zanos TP, Marmarelis VZ, Ojemann GA & Fetz EE (2012). Relationships between spike-free local field potentials and spike timing in human temporal cortex. *J Neurophysiol* **107**, 1808–1821.

Zanos TP, Mineault PJ & Pack CC (2011). Removal of spurious correlations between spikes and local field potentials. *J Neurophysiol* **105**, 474–486.

Zhuang J, Truccolo W, Vargas-Irwin C & Donoghue JP (2010). Decoding 3-D reach and grasp kinematics from high-frequency local field potentials in primate primary motor cortex. *IEEE Trans Biomed Eng* **57**, 1774–1784.

Additional information

Author contributions

All authors designed and conceived the experiments, collected and interpreted the data and wrote the article. S.W. analysed the data. All authors approved the final version. Experiments were performed at the Sobell Department of Motor Neuroscience and Movement Disorders, UCL Institute of Neurology, London, UK.

Competing interests

None.

Funding

This study was supported by the Wellcome Trust and a Marie Curie Postdoctoral Fellowship (S.W.).

Acknowledgements

We thank Sam Shepherd, Lianne McCombe, Spencer Neal, Dan Voyce, Victor Baller, Jonathan Henton, Dave Thomas, Xavier Golay and Martin Lawton for technical support. Roland Philipp and Ganesh Vigneswaran assisted with recordings.